2024 IEEE International Conference on Robotics and Automation (ICRA 2024)
May 13-17, 2024. Yokohama, Japan

Automated Sperm Immobilization with a Clinically-Compatible and Compact XYZ Stage

Haocong Song[1*], Wenyuan Chen[1*], Changsheng Dai[2], Guanqiao Shan[1], Steven Yang[1], Aojun Jiang[1], Zhuoran Zhang[3], and Yu Sun[1]

***Abstract*— Automated positioning systems play a pivotal role in micro-scale cell manipulation. In clinical intracytoplasmic sperm injection (ICSI) of in vitro fertilization (IVF) treatment, a motile sperm needs to be immobilized by glass micropipette tapping for subsequent surgical steps. The process requires accurate tracking of the target sperm and precise alignment between the sperm tail and the micropipette. Manual sperm immobilization suffers from inconsistent success rates, and current robotic systems developed for the task fail to comply with the standard clinical setup. Instead of using a motorized micromanipulator as in existing robotic systems, this paper presents an automated, compact three-dimensional positioning stage for sperm immobilization that can be seamlessly integrated into standard clinical platforms. Based on the analysis of the sperm head orientation, an adaptive tail tapping planning strategy is established to avoid the risk of touching the sperm head where DNA is contained. A visual servo controller equipped with a dynamic sperm motion observer is employed to achieve precise tracking and positioning of the target sperm three-dimensionally. Experimental results revealed the system achieved a success rate of 93.5% and a time cost of 5.5 s for automated sperm immobilization.**

I. Introduction

Accurate positioning systems have wide applications in cell manipulation such as in vitro fertilization (IVF) [1], cell cloning [2], and mitochondria disease treatment [3]. It is crucial to precisely move a target cell to a desired position for executing manipulation tasks such as injection [4], enucleation[5], and biopsy[6]. An example application of cell manipulation is the robotic immobilization of a motile sperm. Sperm immobilization is a critical step in intracytoplasmic sperm injection (ICSI) [7], the most widely used surgical treatment for IVF. The primary goal of immobilizing a motile sperm is to prevent the disturbance from tail beating inside the oocyte after injection[8].

Conventional sperm immobilization is performed by embryologists who operate a hydraulically-driven micromanipulator to move a glass micropipette to tap the sperm tail against the substrate[9], thereby breaking the sperm tail membrane and motor proteins. The procedure requires the accurate positioning of the target sperm in the microscope's field of view (FOV), and the precise alignment of the micropipette's tip with the tapping spot on the sperm tail. At present, clinical practice relies on manual stages for sperm positioning, which suffers from limited accuracy [10]. Given the agility of a healthy sperm (i.e., swimming speed >20 μm/s, wiggling frequency 5-10 Hz) [11], manual operation is skill dependent, and success rates vary across operators.

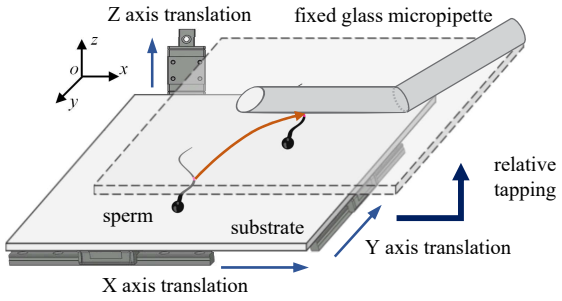

Fig. 1. Schematic illustration of the developed three-dimensional positioning system for sperm immobilization. Different from previously reported robotic sperm immobilization systems, the glass micropipette is fixed during the entire process. Immobilization is performed by controlling the motions of the compact XYZ positioning stage that fits seamlessly with a standard clinically used manual microscope stage.

To minimize human involvement and automate the process, robotic sperm immobilization was attempted in [12] and [13]. Motorized stages with direct current (DC) motors were developed for sperm positioning at the micrometer scale. However, the motorized stages can only provide two degrees of freedom (DOF) in the X-Y plane [14], [15]. Motorized micromanipulators are required to execute sperm tail tapping in the three-dimensional space. In addition, the DC-driven XY stages are bulky and require the removal of the manual microscope stage for motorized X-Y positioning, interfering with the standard setup in IVF clinics.

Compared to other types of motors, piezoelectric positioners [16] are much smaller in size and have sub-micrometer positioning accuracies. Leveraging these advantages, the use of piezoelectric positioners enables the construction of compact XYZ stages that can be readily placed on a standard manual microscope stage. Such a stage can be controlled three-dimensionally to perform sperm immobilization by elevating the substrate through the Z axis motion (Fig. 1), freeing the need for a motorized micromanipulator that is not typically used in standard clinical setups.

When the XYZ stage moves upwards for contacting the sperm with the micropipette tip for sperm immobilization, the sperm deviates from the initial focal plane (Fig. 2(c)&(d)) as the substrate is elevated by the stage. Out-of-focus imaging poses challenges in the accurate tracking of the

[1]Robotics Institute, University of Toronto, Canada. [2]School of Mechanical Engineering, Dalian University of Technology, China. [3]School of Science and Engineering, The Chinese University of Hong Kong (Shenzhen), China. *These authors contributed equally to this work.
Corresponding authors: Changsheng Dai (daichangsheng@dlut.edu.cn); Yu Sun (sun@mie.utoronto.ca).

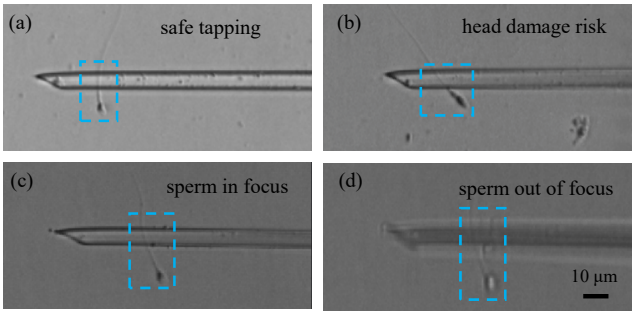

Fig. 2. (a) Ideal tail tapping is when the sperm's swimming direction is nearly perpendicular to the micropipette. (b) For a sperm swimming in other directions relative to the micropipette, tapping risks damaging the sperm head where DNA is contained. (c) Before tapping, the sperm is visually servoed to the target position with the sperm in focus. (d) For tapping, the sperm becomes out-of-focus when the substrate is moved upwards against the micropipette. Scale bar: 10 μm.

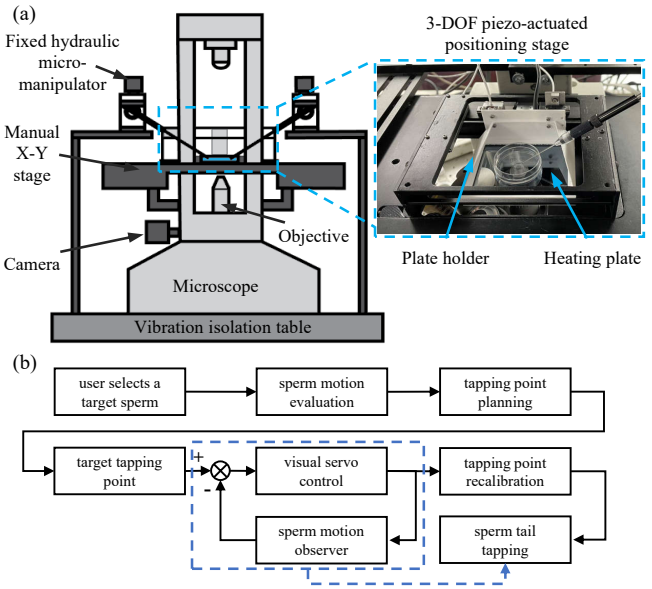

Fig. 3. (a) System setup. The XYZ piezoelectric motors-driven stage is seamlessly integrated into the microscope's manual stage. A heating plate is assembled on the plate holder to maintain sperm viability in the Petri dish at room temperature. (b) The automated sperm immobilization workflow begins with user selection and pre-evaluation of a target sperm. Subsequently, the tapping point on the sperm tail is determined based on the sperm orientation. The sperm tail is then visually servoed to the target position beneath the micropipette. The tapping point on the sperm tail is further adjusted before micropipette tapping.

sperm, potentially causing misalignments between the sperm tail and the target tapping position before the micropipette tip contacts the substrate. To handle out-of-focus imaging, feedforward methods in visual servo control were adopted for error compensation in cell positioning [17], [18]. However, these approaches were designed for objects with constant velocities while sperm exhibits dynamic motions.

Another challenge is that tail tapping on sperm swimming in directions not perpendicular to the micropipette (Fig. 2(a)&(b)) risks damaging the sperm head that contains DNA. The wiggling motion of the sperm head [19] can lead to collisions with the micropipette if the tapping point is not properly selected. To address this challenge, methods have been developed to adjust the sperm swimming direction [13], [20] to the perpendicular direction. However, these approaches rely on devices such as rotational stages and motorized micromanipulators that are not compatible with the clinical setup. Laser heating [21] and piezo vibration [22] were also attempted to ablate the tail membrane other than micropipette tapping. However, their indirect influence on the sperm's DNA integrity remains unknown.

This paper presents an automated three-dimensional positioning system that is capable of immobilizing motile sperm with a clinically compatible, compact XYZ stage. To mitigate the risk of sperm head damage during tapping, an adaptive planning strategy of the sperm tail tapping point is established based on the sperm orientation analysis. To minimize the error introduced by out-of-focus imaging and thus ensure accurate sperm positioning, a sperm motion observer is adapted to compensate for the dynamic sperm movement. The system achieved higher accuracy in sperm positioning and better compatibility than previously reported robotic sperm immobilization [12], [17]. Experimental results demonstrated a sperm immobilization success rate of 93.5% (n=200 sperm) and a time cost of 5.5 s.

II. System Overview

A. System Setup

The system setup, as shown in Fig. 3(a), comprises an inverted microscope integrated with the portable XYZ piezoelectric motors-driven stage directly placed on the microscope's manual stage. The hydraulic micromanipulator is manually controlled with a clinical standard micropipette (MIC-50-35, Origio) mounted on the hydraulic micromanipulator. For sperm immobilization, the positioning of the hydraulic micromanipulator is fixed, and the XYZ stage moves the cell plate to contact the target sperm's tail with the micropipette tip for tapping. Visual feedback is provided by a camera connected to the microscope that captures images at 1200 $\times$ 900 pixels and a frame rate of 30 frames per second, which is sufficient for tracking sperm tails whose beating frequency is 5-10 Hz [23].

The workflow of the sperm immobilization process is summarized in Fig. 3(b). The target sperm is selected via the user interface of our software. The system then derives the target point for tapping on the sperm tail from the sperm position and orientation measurement. Next, visual servo control is engaged to position the sperm to the target position near the micropipette's tip, during which a sperm motion observer is employed to compensate for the sperm motion. If the sperm's orientation varies, the tapping point is recalibrated and adjusted prior to micropipette tapping. Once the tapping point on the tail is accurately aligned with the micropipette, the micropipette tapping is executed

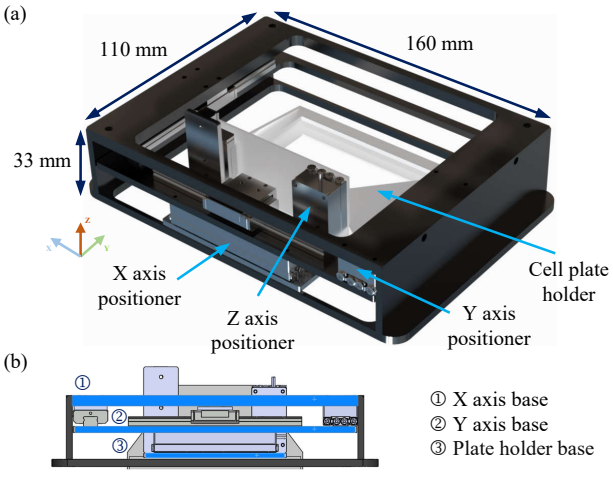

Fig. 4. (a) The compact piezoelectric motors-driven XYZ stage. (b) The positioners of the Y and X axes are mounted below the top base and the middle base. The cell plate holder is mounted on the bottom base such that cells are within the depth field of the microscope objectives.

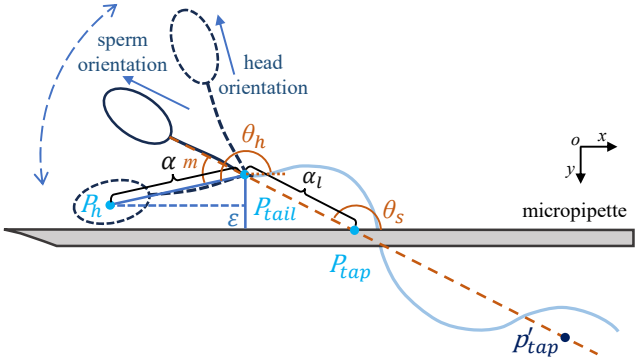

Fig. 5. Geometric model of sperm head oscillating motion and tapping point planning scheme. The sperm head position P_h is the centroid of the segmented oval shape. The tail position P_{tail} is obtained by extending the major axis of the sperm head by the length of α. By modeling the periodic oscillating motion of the sperm head, the sperm orientation θ_s is decoupled from the head orientation θ_h. The tapping point P_{tap} is fitted by translating P_{tail} with α_l along θ_s. P'_{tap} is the infeasible tapping point for certain situations.

through the motion of the positioning stage. The stage is controlled to move upwards for a predefined distance that exceeds the original height of the micropipette above the substrate. Throughout the tapping process, visual servoing continues to be effective in maintaining the sperm tail at the desired position.

B. Piezoelectric Motors-Driven Stage Design

As shown in Fig. 4(a), the stage is designed for integration into a standard microscope platform to provide accurate positioning of cells. Unlike conventional motorized stages used on microscopes that only offer motions in the X and Y axes, our design implements 3 DOFs, enabling translational movements along all the X, Y, and Z axes. Two piezoelectric actuators (LS-1760, NATORS Ltd.) are used for X and Y positioning, providing a travel range of 61 mm with positioning resolutions of 10 nm. The Z axis is equipped with a short-range actuator (LS-1730, NATORS Ltd.) that offers a travel range of 31 mm also with a positioning resolution of 10 nm. To ensure that the specimen lies within the maximal focal range of the microscope's objective, the positioners of the X and Y axes are mounted upside down. With this configuration (see Fig. 4(b)), the stage generates motions in the X and Y axes below the mounting base.

III. Methods

A. Automated Tapping Point Planning

The conventional tail tapping-based robotic sperm immobilization system [12] executes micropipette tapping on a fixed position relative to the sperm head position (Fig. 2(a)). For sperm swimming in directions other than near perpendicular to the micropipette (Fig. 2(b)), the wiggling motion of the sperm head [19] (Fig. 5) can lead to possible collision during tapping. To solve this issue, the tapping point P_{tap} on the sperm tail needs to be dynamically planned according to varying sperm orientations.

To analyze the pattern of sperm orientation, the target sperm is first detected and tracked using the algorithms developed in our previous studies [13] and [24] to obtain the sperm head position $P_{head} = [x_{head}, y_{head}]^T$. Assuming that the major axis of the head is aligned with the major axis of the rigid midpiece [25], the sperm tail position $P_{tail} = [x_{tail}, y_{tail}]^T$ is derived according to the coordinate system in Fig. 6

$$\begin{bmatrix} x_{tail} \\ y_{tail} \end{bmatrix} = \begin{bmatrix} x_{head} \\ y_{head} \end{bmatrix} + \alpha \begin{bmatrix} -\cos\theta_h \\ \sin\theta_h \end{bmatrix} \tag{1}$$

where α is a scalar value determining the spatial distance between the head centroid and the estimated P_{tail}, and θ_h is the head orientation that represents the anticlockwise angle between the sperm head major axis and the X axis (Fig. 5). In our experiments, α was set as 10 μm.

To establish a tapping point planning scheme, the sperm orientation θ_s is defined as the angle between the X axis and the central axis around which the sperm head oscillates, thereby needing to be decoupled from θ_h. The wiggling pattern of motile sperm is analyzed in [26], where the periodic sperm head orientation is modeled as

$$\theta_h = A\sin(\cdot) + \theta_s \tag{2}$$

where A is the oscillation amplitude derived from visual feedback.

To prevent the physical contact between the micropipette and the sperm head due to its oscillation, the constraint must be met as

$$|P_{tail} - P_{tap}|_y > \alpha \cdot \sin\theta_{hm} \tag{3}$$

where $\theta_{hm} = \theta_s \pm A$ is the peak angles that the sperm head can reach during the oscillation period. Applying the constraint (3), the scalar distance α_l between the tapping point and the tail position P_{tail} is estimated as

$$\alpha_l = \frac{\alpha \cdot \sin\theta_{hm} + \varepsilon}{\sin\theta_s} \tag{4}$$

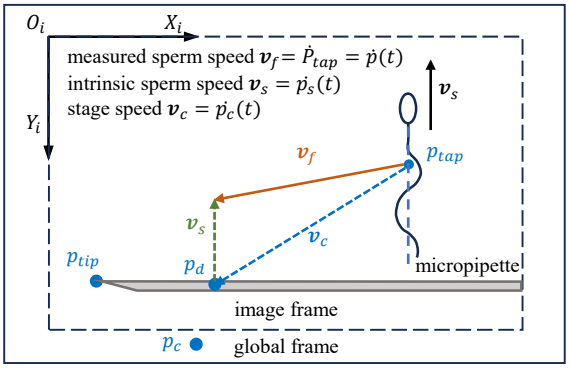

Fig. 6. Schematic diagram of spatial positions. P_c is any reference point on the stage moving in the global frame. The sperm velocity from visual feedback v_f is the vector sum of the stage velocity v_c and the intrinsic sperm velocity v_s. P_d is the target tapping point on the micropipette, which is 60 μm to the right of the micropipette's tip P_{tip}.

where ε is a slack variable that ensures a marginal distance between the edge of the sperm head and the micropipette. In our experiment, ε was set as 5 μm. Applying α_l on P_{tail} along the sperm orientation axis, the tapping point P_{tap} is obtained as

$$P_{tap} = P_{tail} + \alpha_l \begin{bmatrix} -\cos\theta_s \\ \sin\theta_s \end{bmatrix} \tag{5}$$

If the calculated α_l is greater than 25 μm, the sperm will be discarded for immobilization as P'_{tap} will be the near end of the sperm major axis (see Fig. 5). The micropipette's tip is likely to fail to tap on the sperm tail because of the wave-like tail motion propagating to the tail end [26]. These cases happen when sperm are swimming in near parallel directions with the micropipette or the sperm head is oscillating at large amplitudes.

B. Visual Servo Controller Design

Different from immobile cells such as oocytes and embryos, a healthy sperm swims fast (>20 μm/s) in the microscope's FOV, requiring visual servoing to position and maintain the target sperm under the micropipette. Furthermore, during the elevation of the substrate to make contact with the micropipette for sperm immobilization, the visual feedback is blurred thereby yielding inaccurate tracking results. Without offsetting the controller output properly, the sperm can easily slip away from the desired position before being immobilized.

To tackle this challenge, a visual servo controller equipped with a dynamic sperm motion observer is developed (Fig. 7). As shown in Fig. 6, P_d is the target position of the sperm tail in the image frame $X_iO_iY_i$. Let $p(t) = P_{tap}$ to be the obtained tapping point on the sperm tail, the objective of visual servoing is to minimize the error $e(t)$

$$e(t) = p(t) - P_d \tag{6}$$

In our experiments, P_d was set to be $P_{tip} + \mathbf{J}[60\,\mu m, 0\,\mu m]^T$, where $\mathbf{J}$ is the image Jacobian matrix.

We define v_c as the controller output, i.e., the velocity of the motorized stage in the global frame (Fig. 6). Assuming

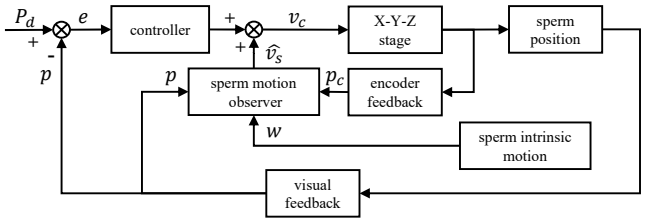

Fig. 7. System control diagram. A Kalman filter-based sperm motion observer is designed to estimate and compensate for the sperm's intrinsic motion v_s during close loop control. The measured sperm movement is calculated from the encoder feedback p_c of the XYZ stage and the visual feedback p of the camera. By evaluating the process noise w introduced by sperm intrinsic motion, $\widehat{v_s}$ is derived and added to the controller output v_c.

that v_c contributes to sperm's motion via sperm medium in the Petri dish without loss, the measured sperm velocity v_f from visual feedback consists of v_c and the sperm's intrinsic velocity v_s (see Fig. 6), which gives

$$\dot{e} = \dot{p} = v_f = \mathbf{J}(v_c + v_s) \tag{7}$$

By applying the exponential decrease $\dot{e} = -\lambda e$ as the control law[27], the controller output v_c can be derived as

$$v_c = -\lambda \mathbf{J}^{-1} e - \widehat{v_s} \tag{8}$$

where $\widehat{v_s}$ is the estimation of v_s. Substituting (8) into (7) gives

$$\dot{e} = -\lambda \mathbf{J}\mathbf{J}^{-1} e + \mathbf{J}(v_s - \widehat{v_s}) \tag{9}$$

To minimize the term $\mathbf{J}(v_s - \widehat{v_s})$ and thus to ensure the error converges to zero, a sperm motion observer shown in Fig. 7 is designed to estimate $\widehat{v_s}$ for velocity compensation.

Since the sperm is in focus while being servoed to the target position, $\widehat{v_s}$ can be simply updated as $\widehat{v_s} = v_f - v_c$. However, the tapping procedure introduces immeasurable error to v_f while the sperm is out-of-focus due to the elevated substrate. Different from the previous feedforward method [17] that the compensated velocity $\widehat{v_s}$ is set as a constant, we now estimate the intrinsic sperm movement in real-time by adapting a Kalman filter-based sperm motion observer. The state variable X_k is defined as the sperm's displacement in the X-Y plane during the k^{th} sampling period. Let v_1 and v_2 be the displacement along the X and Y direction, $X_k = [v_1, v_2]^T$ is given as

$$X_k = \dot{p}_s(t)|_{t=k} = p_s(k) - p_s(k-1) \tag{10}$$

where $p_s(t)$ is the sperm tail position decoupled from the stage position $p_c(t)$. The decoupling process is given as

$$p_s(t) = p(t) - p_c(t) \tag{11}$$

where $p_c(t)$ is the stage position based on the encoder feedback. The a prior state $X_{k|k-1}$ is modeled as

$$X_{k|k-1} = I_2 X_{k-1|k-1} + w_{k-1} \tag{12}$$

where the state transition matrix I_2 is a 2×2 identity matrix, and w_{k-1} is the process noise as $w_{k-1} \sim \mathcal{N}(0, Q)$. To further estimate the covariance matrix Q which represents the variability of intrinsic sperm velocity, the selected motile

sperm is evaluated for 2 s (60 image frames) while the XYZ stage remains stationary. The estimated covariance matrix $\widehat{Q}$ is calculated as

$$\widehat{Q} = \frac{1}{N-1}\sum_{i=1}^{N}(X_i-\overline{X})(X_i-\overline{X})^{\mathrm{T}} = \frac{1}{N-1}\sum_{i=1}^{N}\begin{bmatrix}(v_{i1}-\overline{v}_1)(v_{i1}-\overline{v}_1) & (v_{i1}-\overline{v}_1)(v_{i2}-\overline{v}_2)\\ (v_{i2}-\overline{v}_2)(v_{i1}-\overline{v}_1) & (v_{i2}-\overline{v}_2)(v_{i2}-\overline{v}_2)\end{bmatrix} \tag{13}$$

where $N = 60$. The posterior state, i.e., the estimated sperm speed $\widehat{v_s}$ at time k is then updated with the current measurement Z_k

$$X_{k|k} = X_{k|k-1} + K_k(Z_k - H_k X_{k|k-1}) \tag{14}$$

where $Z_k = HX_k$, K_k is the Kalman gain, and H_K is the observation matrix.

IV. Experimental Results and Discussion

Human sperm used in the experiments were obtained from the CReATe Fertility Centre in Toronto where all participants provided informed consent. Following the standard clinical practice, fresh human sperm was deposited on a culture dish containing a droplet of culture medium (5 μL PVP solution with HSA, Irvine Scientific) covered by mineral oil to prevent evaporation.

A. Results of Tapping Point Planning

To validate the effectiveness of the tapping point planning strategy, motile sperm were categorized into five groups with swimming directions θ from 90° to 0° relative to the X axis (see Table I). For each group, 50 sperm were selected to be positioned at the target spot near the micropipette tip with both tapping point configurations. The sperm head was observed under the microscope at 20× magnification. If the head pixels exhibit intersections with the pixels of the micropipette, the sperm head was considered to have physical contact with the micropipette.

The quantitative results of the tapping point planning are summarized in Table I, where sperm without head contact was counted for each group. For conventional immobilization with a fixed tapping point on the sperm tail [12], [13], the head avoidance rate remained at 96% (48/50) for sperm with swimming directions $90° \geq \theta > 75°$, but dropped significantly for sperm with $\theta \leq 75°$. The drop occurred because the sperm's wiggling amplitude could easily exceed the predefined distance along the Y axis between the sperm head and the micropipette. In contrast, the adaptive planning strategy achieved a constant head avoidance rate of 96% (144/150) for sperm with swimming directions $\theta \geq 45°$. However, there were some failure cases due to inaccuracies in measuring the sperm's wiggling amplitude A. The head avoidance rate with the planning strategy inevitably dropped below 80% when $\theta < 45°$. In such instances, the sperm was deemed unsuitable for immobilization since the calculated tapping point was near or beyond the end of the sperm tail.

TABLE I
QUANTITATIVE RESULTS OF TAPPING POINT PLANNING

Method	Sperm Swimming Direction θ				
	(75°, 90°)	(60°, 75°)	(45°, 60°)	(30°, 45°)	(0°, 30°)
Fixed	48	42	31	15	0
Planned	50	49	45	40	30

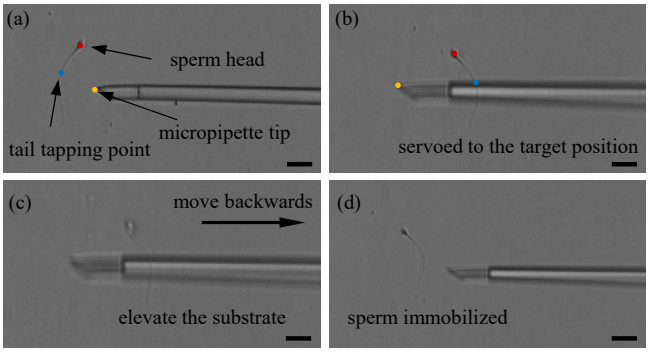

Fig. 8. Automated sperm immobilization. (a) After the target sperm is selected, the sperm is visually tracked by the system. The tail tapping point is derived from the sperm head position and sperm orientation. (b) The sperm is visually servoed to the target position under the micropipette by the positioning stage. (c) The tapping process is achieved by moving the stage upwards and backwards to ablate the tail membrane. (d) The sperm is immobilized. Scale bar: 10 μm.

B. Performance of Visual Servoing

As shown in Fig. 8, the visual servoing process for sperm immobilization consisted of two stages. First, the positioning stage was controlled to position the selected sperm (Fig. 8(a)) to the target tapping spot under the micropipette tip (Fig. 8(b)). Second, the visual servo controller maintained the sperm tail at the target position until the substrate made contact with the stationary micropipette tip (Fig. 8(c)). Visual servoing stopped after the sperm tail was tapped against the substrate, and the stage moved along the X axis to ablate the tail membrane.

To evaluate the performance of the visual servo controller and the sperm motion observer described in Section III-B, two control schemes (dynamic $\widehat{v_s}$ vs. constant $\widehat{v_s}$ [17]) were applied on the same sperm ($\theta_s \approx 45°, v_s \approx 20\,\mu$m/s) for positioning error evaluation. In this experiment, the micropipette was not mounted to tap against the sperm tail since the motility of the same sperm needed to be maintained for repetitive trials. The error curves in Fig. 9(a) show that the controller with motion observer converged faster with less disturbance during positioning. This is due to the dynamic sperm movement was offset by the designed sperm motion observer. For the tapping part, when the stage intentionally altered the Z position to move the sperm out-of-focus, both curves exhibited a considerable deviation from the stable state (30 pixels vs. 50 pixels). However, the controller with motion observer was able to restore the stable state in 0.5 s while the controller without the motion observer had an average error of 25 pixels. These results confirmed that the

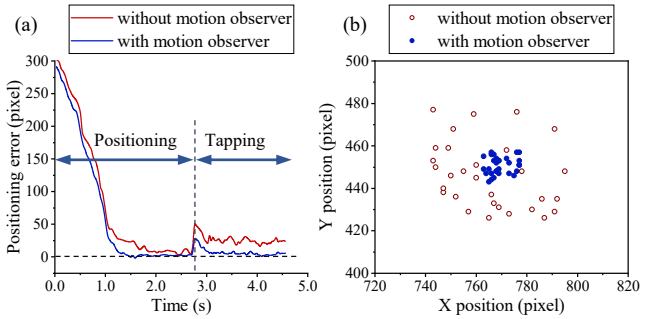

Fig. 9. (a) Positioning error of a target sperm during visual servoing. The first stage of visual servoing was to position the sperm to the tapping point. The second phase aimed to maintain the sperm's position until the tail was tapped against the stationary/fixed micropipette tip. (b) Sperm positions in the image frame after visual servoing. The target position of the FOV (P_d) was (770, 450).

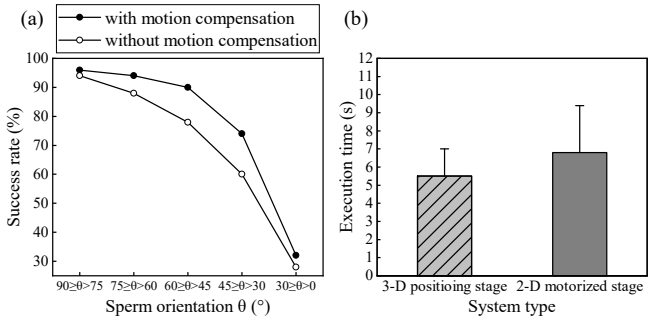

Fig. 10. (a) Sperm immobilization success rate according to the sperm swimming direction θ ($\theta = \theta_s$, when $0^\circ < \theta_s \leq 90^\circ$; $\theta = 180^\circ - \theta_s$, when $90^\circ < \theta_s \leq 180^\circ$). (b) Performance comparison between the developed three-dimensional positioning system and the conventional 2-DOF motorized stage with a motorized micromanipulator for automated sperm immobilization.

sperm motion observer successfully corrected the error posed by out-of-focus imaging.

In addition to positioning error curve analysis, 60 sperm (30 in each group) were selected for examining the final positions after visual servoing. The results shown in Fig. 9(b) confirmed that the controller with motion observer performed significantly better than the original controller (2.3 ± 1.2 μm vs. 10.2 ± 3.4 μm, $p < 0.05$). Note that the positioning error was converted from pixels to micrometers according to microscope calibration.

C. Success Rate of Sperm Immobilization

The complete process of sperm immobilization conducted with the developed three-dimensional positioning system is shown in Fig. 8. Using the sperm tail tapping planning strategy established in Section III-A, the immobilization success rate was measured for different sperm swimming directions and visual servo strategies. Immobilization was considered successful when the target sperm lost its motility after the immobilization process.

The sperm categorization followed the same configuration in Section IV-A. For each group, 100 sperm were selected to conduct immobilization using the visual servo control while 50 with the dynamic motion compensation method and the other 50 not. The experimental results showed that the system with the sperm motion observer performed better than that without the motion observer on sperm swimming in all directions (77.2% vs. 68.6%). For visual servo with dynamic motion compensation, the best performance was achieved on sperm of $90^\circ \geq \theta > 75^\circ$ with a success rate of 96% (48/50). In addition, as shown in 10(a), the success rate of the controller with motion observer remained steady for θ varying from 90° to 45° (from 96% to 90%), while the success rate of the original controller dropped from 94% to 78%. The immobilization success rate of both strategies dropped significantly for sperm with $\theta \leq 45^\circ$. In these instances, the estimated tapping spot was near the end of the sperm tail, making it challenging for precise micropipette contact with the sperm tail due to its oscillation. As a result, sperm swimming in directions with $\theta > 45^\circ$ relative to the micropipette's axis were recommended for immobilization by the system, yielding an average success rate of 93.3% (140 out of 150).

To compare the system performance with previously reported robotic immobilization using a 2-DOF motorized stage and a motorized micromanipulator [12], 100 sperm (50 in each group) with favored swimming directions ($\theta > 45^\circ$) were selected for immobilization. As shown in Fig. 10(b), both groups achieved a high success rate (94% vs. 96%). The results contributed to a combined success rate of 93.5% (187 out of 200, $\theta > 45^\circ$) of the developed system. For each sperm, the average time cost of the whole immobilization process with the compact XYZ positioning stage was 5.5 ± 1.5 s, on par with the conventional robotic system employing an XY motorized stage and a motorized micromanipulator that operated at 6.8 ± 2.6 s. The developed XYZ stage was more time efficient as it continuously completed all procedures through the stage motion alone. In contrast, the conventional system relied on the collaboration between the XY stage and the micromanipulator, leading to comparatively longer processing time. However, it is noteworthy that the major highlight of our developed system lies in its clinical compatibility rather than time efficiency.

V. Conclusion

This paper presented an automated three-dimensional positioning system for cell manipulation with robotic sperm immobilization as an illustrative application. The system integrated three piezo-actuated positioners within a compactly designed structure, offering 3 DOFs along the X, Y, and Z axes. The need for adding a motorized micromanipulator to execute sperm tail tapping was eliminated. The established tail tapping planning strategy was effective in avoiding physical contact between the sperm head and the micropipette tip. A visual servo controller, aided by a sperm motion observer, was employed to achieve precise positioning of the target sperm with an accuracy of 2.3 μm. Experiments on 200 sperm revealed a success rate of 93.5% for immobilization and a time cost of 5.5 s. The compatibility with standard clinical setups can facilitate its adoption for clinical application.

REFERENCES

[1] B. J. Van Voorhis, "In vitro fertilization," *New England Journal of Medicine*, vol. 356, no. 4, pp. 379–386, 2007.

[2] Z. Liu, Y. Cai, Y. Wang, Y. Nie, C. Zhang, Y. Xu, X. Zhang, Y. Lu, Z. Wang, M. Poo *et al.*, "Cloning of macaque monkeys by somatic cell nuclear transfer," *Cell*, vol. 172, no. 4, pp. 881–887, 2018.

[3] E. Kang, J. Wu, N. M. Gutierrez, A. Koski, R. Tippner-Hedges, K. Agaronyan, A. Platero-Luengo, P. Martinez-Redondo, H. Ma, Y. Lee *et al.*, "Mitochondrial replacement in human oocytes carrying pathogenic mitochondrial dna mutations," *Nature*, vol. 540, no. 7632, pp. 270–275, 2016.

[4] Y. Sun and B. J. Nelson, "Biological cell injection using an autonomous microrobotic system," *The international journal of robotics research*, vol. 21, no. 10-11, pp. 861–868, 2002.

[5] Q. Zhao, J. Qiu, Z. Feng, Y. Du, Y. Liu, Z. Zhao, M. Sun, M. Cui, and X. Zhao, "Robotic label-free precise oocyte enucleation for improving developmental competence of cloned embryos," *IEEE Transactions on Biomedical Engineering*, vol. 68, no. 8, pp. 2348–2359, 2020.

[6] G. Shan, C. Dai, H. Liu, X. Wang, W. Dou, C. Ru, Z. Zhang, and Y. Sun, "Robotic blastocyst biopsy," *IEEE/ASME Transactions on Mechatronics*, 2022.

[7] P. Rubino, P. Viganò, A. Luddi, and P. Piomboni, "The icsi procedure from past to future: a systematic review of the more controversial aspects," *Human reproduction update*, vol. 22, no. 2, pp. 194–227, 2016.

[8] G. D. Palermo, P. N. Schlegel, L. T. Colombero, N. Zaninovic, F. Moy, and Z. Rosenwaks, "Aggressive sperm immobilization prior to intracytoplasmic sperm injection with immature spermatozoa improves fertilization and pregnancy rates," *Human Reproduction*, vol. 11, no. 5, pp. 1023–1029, 1996.

[9] A. Velaers, G. Paternot, S. Debrock, T. DHooghe, and C. Spiessens, "Triple touch sperm immobilization vs. single touch sperm immobilization in icsi-a randomised trial," *Reproductive Biology and Endocrinology*, vol. 10, no. 1, pp. 1–6, 2012.

[10] G.-Y. Gu, L.-M. Zhu, C.-Y. Su, H. Ding, and S. Fatikow, "Modeling and control of piezo-actuated nanopositioning stages: A survey," *IEEE Transactions on Automation Science and Engineering*, vol. 13, no. 1, pp. 313–332, 2014.

[11] T. G. Cooper and C.-H. Yeung, "Computer-aided evaluation of assessment of grade a spermatozoa by experienced technicians," *Fertility and sterility*, vol. 85, no. 1, pp. 220–224, 2006.

[12] C. Leung, Z. Lu, N. Esfandiari, R. F. Casper, and Y. Sun, "Automated sperm immobilization for intracytoplasmic sperm injection," *IEEE Transactions on Biomedical Engineering*, vol. 58, no. 4, pp. 935–942, 2010.

[13] Z. Zhang, C. Dai, J. Huang, X. Wang, J. Liu, C. Ru, H. Pu, S. Xie, J. Zhang, S. Moskovtsev *et al.*, "Robotic immobilization of motile sperm for clinical intracytoplasmic sperm injection," *IEEE Transactions on Biomedical Engineering*, vol. 66, no. 2, pp. 444–452, 2018.

[14] B. Tamadazte, N. L.-F. Piat, and S. Dembélé, "Robotic micromanipulation and microassembly using monoview and multiscale visual servoing," *IEEE/ASME Transactions on Mechatronics*, vol. 16, no. 2, pp. 277–287, 2010.

[15] X. Liu, Z. Lu, and Y. Sun, "Orientation control of biological cells under inverted microscopy," *IEEE/ASME Transactions on Mechatronics*, vol. 16, no. 5, pp. 918–924, 2010.

[16] C. Zhou, Z. Gong, B. K. Chen, Z. Cao, J. Yu, C. Ru, M. Tan, S. Xie, and Y. Sun, "A closed-loop controlled nanomanipulation system for probing nanostructures inside scanning electron microscopes," *IEEE/ASME Transactions on Mechatronics*, vol. 21, no. 3, pp. 1233–1241, 2016.

[17] Z. Zhang, C. Dai, X. Wang, C. Ru, K. Abdalla, S. Jahangiri, C. Librach, K. Jarvi, and Y. Sun, "Automated laser ablation of motile sperm for immobilization," *IEEE Robotics and Automation Letters*, vol. 4, no. 2, pp. 323–329, 2019.

[18] Y. Guan, T. Xu, J. Liu, and X. Wu, "Image-based visual servoing of helical microswimmers for arbitrary planar path following at low reynolds numbers," in *2017 IEEE/RSJ International Conference on Intelligent Robots and Systems (IROS)*. IEEE, 2017, pp. 1883–1888.

[19] J. F. Jikeli, L. Alvarez, B. M. Friedrich, L. G. Wilson, R. Pascal, R. Colin, M. Pichlo, A. Rennhack, C. Brenker, and U. B. Kaupp, "Sperm navigation along helical paths in 3d chemoattractant landscapes," *Nature communications*, vol. 6, no. 1, p. 7985, 2015.

[20] C. Dai, G. Shan, H. Liu, C. Ru, and Y. Sun, "Robotic manipulation of sperm as a deformable linear object," *IEEE Transactions on Robotics*, vol. 38, no. 5, pp. 2799–2811, 2022.

[21] L. M. Davidson, Y. Liu, T. Griffiths, C. Jones, and K. Coward, "Laser technology in the art laboratory: a narrative review," *Reproductive biomedicine online*, vol. 38, no. 5, pp. 725–739, 2019.

[22] C. Dai, S. Zhuang, G. Shan, H. Liu, Y. Wang, C. Ru, and Y. Sun, "Automated piezo-assisted sperm immobilization," *IEEE Transactions on Automation Science and Engineering*, 2023.

[23] E. A. Gaffney, H. Gadêlha, D. J. Smith, J. R. Blake, and J. C. Kirkman-Brown, "Mammalian sperm motility: observation and theory," *Annual Review of Fluid Mechanics*, vol. 43, pp. 501–528, 2011.

[24] C. Dai, Z. Zhang, J. Huang, X. Wang, C. Ru, H. Pu, S. Xie, J. Zhang, S. Moskovtsev, C. Librach *et al.*, "Automated non-invasive measurement of single sperms motility and morphology," *IEEE Transactions on Medical Imaging*, vol. 37, no. 10, pp. 2257–2265, 2018.

[25] H. Miyata, Y. Satouh, D. Mashiko, M. Muto, K. Nozawa, K. Shiba, Y. Fujihara, A. Isotani, K. Inaba, and M. Ikawa, "Sperm calcineurin inhibition prevents mouse fertility with implications for male contraceptive," *Science*, vol. 350, no. 6259, pp. 442–445, 2015.

[26] C. Dai, G. Shan, X. Liu, C. Ru, L. Xin, and Y. Sun, "Automated orientation control of motile deformable cells," *IEEE Transactions on Automation Science and Engineering*, 2022.

[27] F. Chaumette and S. Hutchinson, "Visual servo control. ii. advanced approaches [tutorial]," *IEEE Robotics & Automation Magazine*, vol. 14, no. 1, pp. 109–118, 2007.